MILITARY TECHNICAL COLLEGE
CAIRO - EGYPT

FINITE ELEMENT ANALYSIS OF MULTI-VENT MULTI-SPAN FOLDED-PLATE STRUCTURES

By
Dr. Sami N. Mikhaiel[1] & Eng. Atef S. Gindy[2]

ABSTRACT

A general finite element computer code for the space analysis of folded-plate structures has been developed based on the stiffness method. A direct access peripheral storage is used as a scratch file in the formulation of the overall stiffness and load matrices. This made it possible to analyze large multi-vent, multi-span, folded-plate structures. The stiffness matrix of a one-dimensional space frame element assuming nodal forces and displacements at the top points of the cross-sections was derived and used for the simulation of edge beams. The triangular plane-stress element was used for modeling the in-plane action of diaphragms.

Check problems of single-vent simply supported folded-plate structures with and without edge beams have been solved assuming infinitely stiff end-diaphragms and the results of both displacements and internal stresses were compared with the available "exact" analytical solution. This showed complete agreement in both displacements and stresses.

Practical examples of three-vent simply supported and continuous folded-plate roofs have been solved. Effect of edge beams and ties were considered. In case of continuous folded-plates, the effect of the inner supports as point supports on the ridges or as a diaphragm supported at the ridge points was considered and discussed. Several practical conclusions have been made.

INTRODUCTION

The ability of folded-plate structures to span large areas without requiring intermediate supports makes them very attractive to the designer. Many authors presented approximate methods for the evaluation of internal stresses in folded-plates. In 1957, an "exact" method based on the theory of elasticity was presented

1) Lecturer, Struct. Eng. Dept., Cairo Univ.

2) Demonstrator, Struct. Eng. Dept., Cairo Univ.

by Goldberg and Leve for the analysis of single-vent simply supported folded-plate roofs. However, the method is considerably complicated for design purposes.

The great progress in the analysis of structures was due to the progress in electronic computers through the last twenty years. In this work, an integrated finite element system for the general analysis of folded-plate structures based on the stiffness method is presented. To overcome the problem of limited computer storage which generally exists in the space analysis of such large structures, a direct access peripheral storage has been used in the system.

The problem formulation, description of stiffness and transformation matrices used, are presented in the next section. A macro flow chart is then given to show the sequence of calculations through the computer system. Check problems of one-vent simply supported folded-plate roofs have been solved and the results obtained are compared to those from the "exact" analytical solution (3). Practical examples of more complicated structures have been solved. Finally, a summary of the main findings is given in the conclusions.

PROBLEM FORMULATION

Stiffness Matrix of a Folded-Plate Element

As this paper is concerned with prismatic folded-plate structures, the rectangular element is used for modeling the space action of these structures. As usual for planer elements, the in-plane and the out-of-plane actions are completely independent. Two in-plane translations u and v at each of the four nodes are considered for the simulation of the in-plane action, whereas, three out-of-plane displacements w, θ_x and θ_y at each of the four nodes are taken for modeling the bending action. Therefore, the stiffness matrix for the plane-stress action is based on the four terms incomplete second order polynomial for both u and v, such that

$$\underset{2x1}{\begin{Bmatrix} u \\ v \end{Bmatrix}} = \underset{2x8}{\begin{bmatrix} 1 & x & y & xy & 0 & 0 & 0 & 0 \\ 0 & 0 & 0 & 0 & 1 & x & y & xy \end{bmatrix}} \underset{8x1}{\{\alpha\}} \quad \ldots\ldots\ldots \quad (1)$$

The stiffness matrix for the bending action is based on the well known twelve terms incomplete fourth order polynomial for w, such that

$$w = \underset{1x12}{\begin{bmatrix} 1 & x & y & x^2 & xy & y^2 & x^3 & x^2y & xy^2 & y^3 & x^3y & xy^3 \end{bmatrix}} \underset{12x1}{\{\alpha\}} \quad \ldots\ldots (2)$$

That is, five degrees of freedom are only considered at each of the nodes. However, for convenience of the overall formulation of the problem, θ_z was taken into account as a displacement component at each of the four nodes. In order to include the θ_z term, which is known to be neglegible and not to affect the

other terms in the element stiffness matrix, the relationship between θ_z and M_z at any of the nodes can be expressed by a "dummy" equation as follows

$$M_z = 0.\theta_z \qquad \ldots\ldots\ldots (3)$$

Therefore, six components of nodal forces and displacements are considered at each of the nodes. Consequently, the stiffness matrix of the folded-plate element is taken of dimensions (24x24). If $[K^p]$ and $[K^b]$ are the (8x8) and (12x12) stiffness matrices representing the plane-stress and bending actions respectively, each of these matrices can be partitioned corresponding to the four nodes of the element. The submatrices in $[K^p]$ will be of dimensions (2x2), while those in $[K^b]$ are of dimensions (3x3). The stiffness matrix of the folded-plate element referred to the local system of axes will therefore be

$$[K_\ell] = \begin{bmatrix}
K^p_{11} & [0] & 0\,0 & & & & & & & & & \\
[0] & K^b_{11} & 0\,0\,0 & & & & & & & & & \\
0\,0 & 0\,0\,0 & 0 & & & & & & & & & \\
K^p_{21} & [0] & 0\,0 & K^p_{22} & [0] & 0\,0 & & & & & & \\
[0] & K^b_{21} & 0\,0\,0 & [0] & K^b_{22} & 0\,0\,0 & & \text{Symmetric} & & & & \\
0\,0 & 0\,0\,0 & 0 & 0\,0 & 0\,0\,0 & 0 & & & & & & \\
K^p_{31} & [0] & 0\,0 & K^p_{32} & [0] & 0\,0 & K^p_{33} & [0] & 0\,0 & & & \\
[0] & K^b_{31} & 0\,0\,0 & [0] & K^b_{32} & 0\,0\,0 & [0] & K^b_{33} & 0\,0\,0 & & & \\
0\,0 & 0\,0\,0 & 0 & 0\,0 & 0\,0\,0 & 0 & 0\,0 & 0\,0\,0 & 0 & & & \\
K^p_{41} & [0] & 0\,0 & K^p_{42} & [0] & 0\,0 & K^p_{43} & [0] & 0\,0 & K^p_{44} & [0] & 0\,0 \\
[0] & K^b_{41} & 0\,0\,0 & [0] & K^b_{42} & 0\,0\,0 & [0] & K^b_{43} & 0\,0\,0 & [0] & K^b_{44} & 0\,0\,0 \\
0\,0 & 0\,0\,0 & 0 & 0\,0 & 0\,0\,0 & 0 & 0\,0 & 0\,0\,0 & 0 & 0\,0 & 0\,0\,0 & 0
\end{bmatrix}_{24\times 24} \qquad (4)$$

Equilibrium Equations

The matrix given by equation (4) in the local coordinate system gives five components of forces only at each of the nodes. However, in the global coordinate system six equilibrium conditions are assembled at each node. Thus, at a junction of two inclined elements, six equations in the fixed coordinate system are formed from ten independent equations in the local systems and this is satisfactory. On the other hand, at a junction of two co-planer elements, since the local coordinate systems of both elements coincide, we get only five independent equations with respect to either the local or the global axes. Thus, although we get six equilibrium equations in the global axes, only five of these equations are independent. This leads to a singular

system of equilibrium equations.

To overcome this situation, the equilibrium equations at a node connecting co-planer elements should be referred to the local system of axes at that node. This gives five equilibrium equations only corresponding to the five nodal forces considered. However, a non-zero value has to be inserted on the diagonal element corresponding to the sixth degree of freedom θ_z at the node in order to get rid of singularity. This means that equilibrium equations at nodes lying on a fold connecting two plates or a plate with an edge beam will be formed with respect to the global axes, while those at any of the interior nodes will be referred to the local system at that node.

Transformation Matrix and Transformed Stiffness Matrix of a General Element

Figure 1 shows a connection between a plate lying in the horizontal plane and another plate making an angle α with the horizontal plane. The global system of axes x,y and z is assumed to coincide with the local axes of the horizontal plane. The local system of axes for a rectangular element in the inclined plane $\bar{x},\bar{y}$ and $\bar{z}$ is shown in the figure. The rotation matrix[R]for the six components of nodal forces or nodal displacements from local to global systems of axes can be put in the form

$$[R]_{6\times6} = \begin{bmatrix} [\bar{R}]_{3\times3} & [0] \\ [0] & [\bar{R}]_{3\times3} \end{bmatrix} \qquad \ldots\ldots\ldots\ldots\ldots (5)$$

in which

$$[\bar{R}]_{3\times3} = \begin{bmatrix} 1 & 0 & 0 \\ 0 & \cos\phi_{y\bar{y}} & \cos\phi_{y\bar{z}} \\ 0 & \cos\phi_{z\bar{y}} & \cos\phi_{z\bar{z}} \end{bmatrix} \qquad \ldots\ldots\ldots\ldots\ldots (6)$$

The transformation matrix [T] of the entire element depends on the position of the element and on its nodes that are considered as interior nodes. As there is no transformation at the interior nodes, the rotation matrix corresponding to any of these nodes will be the identity matrix $[I]_{6\times6}$ instead of the matrix $[R]_{6\times6}$. Therefore, the transformation matrix [T] of the entire element is a diagonal matrix composed of four diagonal submatrices. Any of these submatrices will be either $[I]_{6\times6}$ if the corresponding node is an interior node, or $[R]_{6\times6}$ if the corresponding node lies on a fold or on a junction with an edge beam. As an example, the transformation matrix for the element shown in Fig. 1 takes the form

6

$$[T] = \begin{bmatrix} [I] & & & 0 \\ & [R] & & \\ & & [R] & \\ 0 & & & [I] \end{bmatrix}_{24x24} \qquad \ldots\ldots\ldots\ldots \quad (7)$$

The transformed stiffness matrix $[K_t]$ of the element is related to its local matrix $[K_\ell]$ in the usual form

$$[K_t] = [T]\,[K_\ell]\,[T]^T \qquad \ldots\ldots\ldots\ldots \quad (8)$$

Diaphragms Modeling

As diaphragms are considered to resist in-plane forces only, they are modeled by plane-stress elements. Herein, the constant strain triangle based on the first order displacement model has been used. For diaphragms lying in the vertical plane y-z (Fig. 2), the displacement components v and w at each of the three corner nodes are considered for the simulation of their in-plane behaviour. Consequently, the stiffness influence coefficients of these elements will correspond only to these two components.

For elements connected to an inclined folded plate, if one or more of the nodes of these elements are connected to interior nodes, the nodal forces of the plane-stress elements and consequently their corresponding stiffness submatrices has to be transformed from the y-z system of axes to the local system of the inclined plate.

The rotation matrix of the two components of nodal forces or displacements from the y-z axes to the $\bar{y}$-$\bar{z}$ axes will be

$$[R]_{2x2} = \begin{bmatrix} \cos\phi_{\bar{y}y} & \cos\phi_{\bar{y}z} \\ \cos\phi_{\bar{z}y} & \cos\phi_{\bar{z}z} \end{bmatrix}_{2x2} \qquad \ldots\ldots\ldots\ldots \quad (9)$$

Thus, the transformation matrix $[T]_{6x6}$ of the entire element is composed of three diagonal submatrices; either $[R]_{2x2}$ or $[I]_{2x2}$. While the submatrix [R] corresponds to the node or the two nodes attached at interior nodes within an inclined plate, the submatrix [I] corresponds to other nodes. As an example, the transformation matrix for the element shown in Fig. 2 is given by

$$[T] = \begin{bmatrix} [R] & & 0 \\ & [I] & \\ 0 & & [I] \end{bmatrix}_{6x6} \qquad \ldots\ldots\ldots\ldots \quad (10)$$

The transformed stiffness matrix of the element $[K_t]$ can be

related to the matrix $[K_g]$ referred to the y-z axes as follows

$$[K_t]_{6x6} = [T]\,[K_g]\,[T]^T \qquad \ldots\ldots\ldots\ldots\ldots \quad (11)$$

Stiffness Matrix of a space Frame Element Having its Nadal Forces and Displacements at the Top Points of the Cross-Sections:

Figure 3 shows a space frame skeletal element with the six components of end-forces {Q} or the end-displacements {q} at either of its two ends are assumed to act at the mid point of the upper edge of the cross-section. The stiffness matrix $[K_\ell]$ of the element has been formulated by the application of the usual principles and is given in equation (12), in which E is Young's modulus ; A is the cross-sectional area; I_y and I_z are the moments of inertia about the y and z axes respectively; J is the torsional moment of inertia; L is the length of the member and h is the depth of its cross-section.

SYSTEM FLOW CHART

As mentioned before, in order to overcome the problem of limited working storage of the computer, the system uses a direct access peripheral storage as a scratch backstore file in the formulation of the overall system of equilibrium equations. The structure is considered to be partitioned into a group of parts. The size of each part depends on the available working storage in the computer. The equilibrium equations corresponding to the nodes within any of these parts is formulated first in the working store, then transmitted to the backstore. The sequence of operations can be illustrated by the macro flow chart given soon in the sequal.

CHECK PROBLEMS

To check the accuracy of the developed system, three test problems given by Goldberg and Leve in reference (3) have been solved. Each of these examples is a one vent simply supported folded-plate roof with infinitely stiff end-diaphragms. Results of the finite element analysis are compared to those given by the "exact" analytical solution in reference (3). Details and results are given below.

Problem 1:

Figure 4 shows the cross-section of a simply supported folded-plate roof with span of 120′ and subjected to the given wind loading. Values of Young's modulus E and Poisson's ratio ν are given as

$$E = 3.7 \times 10^6 \text{ psi} = 5.328 \times 10^8 \text{ lb/ft}^2. \;, \quad \nu = 0.20$$

Table 1 gives the displacement components at the four ridge

$$[K_\ell] = \begin{array}{c|cccccccccccc}
 & 1 & 2 & 3 & 4 & 5 & 6 & 7 & 8 & 9 & 10 & 11 & 12 \\
\hline
1 & \frac{EA}{L} & & & & & & & & & & & \\
2 & 0 & \frac{12\,EI_z}{L^3} & & & & & & & & & & \\
3 & 0 & 0 & \frac{12\,EI_y}{L^3} & & & & & & & & & \\
4 & 0 & \frac{6EI_z h}{L^3} & 0 & \frac{GJ}{L}+\frac{3EI_z h^2}{L^3} & & & & & & & & \\
5 & -\frac{EAh}{2L} & 0 & -\frac{6EI_y}{L^2} & 0 & \frac{4EI_y}{L}+\frac{EAh^2}{4L} & & & & & & & \\
6 & 0 & \frac{6EI_z}{L^2} & 0 & \frac{3EI_z h}{L^2} & 0 & \frac{4\,EI_z}{L} & & & & & & \\
7 & -\frac{EA}{L} & 0 & 0 & 0 & \frac{EA\,h}{2\,L} & 0 & \frac{EA}{L} & & & & & \\
8 & 0 & -\frac{12EI_z}{L^3} & 0 & -\frac{6EI_z h}{L^3} & 0 & -\frac{6EI_z}{L^2} & 0 & \frac{12EI_z}{L^3} & & & & \\
9 & 0 & 0 & -\frac{12EI_y}{L^3} & 0 & \frac{6EI_y}{L^2} & 0 & 0 & 0 & \frac{12EI_y}{L^3} & & & \\
10 & 0 & -\frac{6EI_z h}{L^3} & 0 & -\frac{GJ}{L}-\frac{3EI_z h^2}{L^3} & 0 & -\frac{3EI_z h}{L^2} & 0 & \frac{6EI_z h}{L^3} & 0 & \frac{GJ}{L}+\frac{3EI_z h^2}{L^3} & & \\
11 & \frac{EAh}{2L} & 0 & -\frac{6EI_y}{L^2} & 0 & \frac{2EI_y}{L}-\frac{EAh^2}{4L} & 0 & -\frac{EAh}{2L} & 0 & \frac{6EI_y}{L^2} & 0 & \frac{4EI_y}{L}+\frac{EAh^2}{4L} & \\
12 & 0 & \frac{6EI_z}{L^2} & 0 & \frac{3EI_z h}{L^2} & 0 & \frac{2EI_z}{L} & 0 & -\frac{6EI_z}{L^2} & 0 & -\frac{3EI_z h}{L^2} & 0 & \frac{4EI_z}{L}
\end{array}$$

Symmetric

(12)

Macro Flow Chart

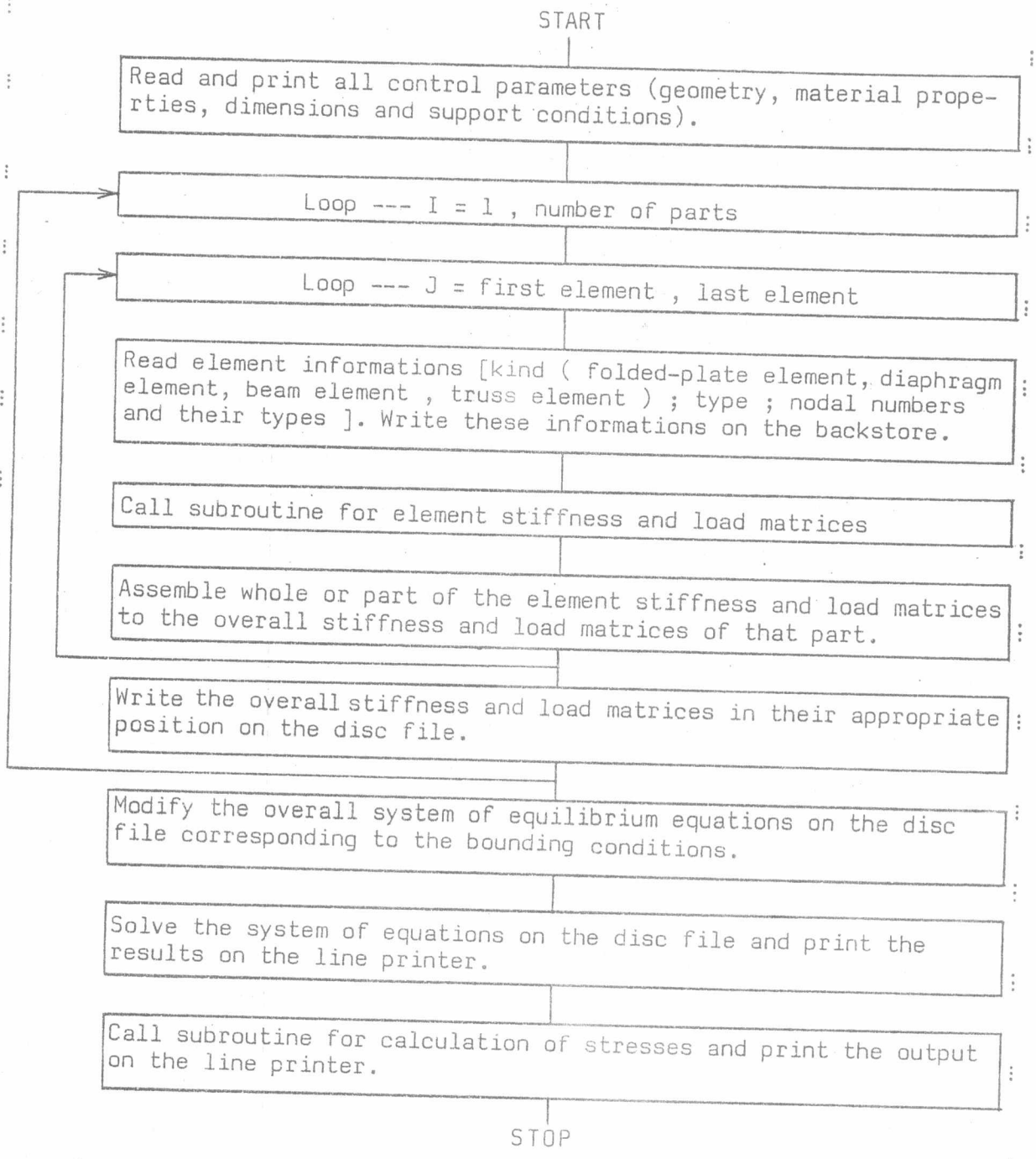

points of the mid-span section. The two in-plane translations v and w at each of the ridge points are referred to the corresponding system of axes at that ridge (Fig.4). First column of the table gives the results of the "exact" analysis according to Leve, whereas the other three columns give the results of the computer analysis using different numbers of elements for modeling one half of the structure only. While the results of the three finite element meshes show the fulfillment of the

Table 1

	Disp. comp.	Exact (Leve)	Finite elements			Units
			154element	48 element	24element	
Ridge point 1	u	- 1.057	- 1.032	- 0.9878	- 0.858	ft.
	v	3.918	3.780	3.6400	2.948	ft.
	w	-224.000	-212.000	-218.1000	-206.700	ft.
	θ_x	- 10.520	- 10.630	- 10.6500	- 10.149	Rad.
Ridge point 2	u	1.193	1.169	1.122	0.986	ft.
	v	- 4.599	- 4.446	- 4.278	- 3.765	ft.
	w	- 7.191	- 6.949	- 6.683	- 5.862	ft.
	θ_x	- 5.465	- 5.085	- 5.045	- 5.001	Rad.
Ridge point 3	u	- 1.0188	- 0.995	- 0.953	- 0.830	ft.
	v	- 4.592	- 4.441	- 4.274	- 3.761	ft.
	w	- 6.059	- 5.845	- 5.604	- 4.859	ft.
	θ_x	1.503	1.429	1.445	1.527	Rad.
Ridge point 4	U	0.715	0.6918	0.656	0.5517	ft.
	v	2.958	2.8490	2.724	2.335	ft.
	w	- 22.090	- 21.9600	- 22.430	- 24.780	ft.
	θ_x	1.161	1.1610	1.168	1.228	Rad.
All values are multiplied by 10^{-4}						

convergence requirement of the numerical solution, there is a very satisfactory agreement in the results of the finest mesh with those of the "exact" solution.

Table 2 gives the "exact" values of some of the internal stresses (the longitudinal normal stress N_x, the longitudinal moment M_x and the transverse moment M_y) at points of the mid-span section (Fig.4) and the corresponding values obtained from the finite element analysis by the three meshes chosen. Again, the convergence requirement is clear and the accuracy is quite satisfactory.

Table 2

N_x lb/ft.	Exact (Leve)	Finite elements 154 Els.	48 Els.	24 Els.	M_x & M_y lb.ft/ft.	Exact (Leve)	Finite elements 154 Els.	48 Els.	24 Els.
N_{x_1}	601.0	585.0	566.78	451.95	M_{x_2}	-44.92	-44.64	-44.43	-43.16
N_{x_2}	-685.0	-668.0	-647.26	-523.1	M_{x_a}	22.42	20.30	-- --	-- --
N_{x_3}	581.0	566.0	547.76	437.97	M_{y_a}	- 3.40	- 3.66	-- --	-- --
N_{x_4}	-408.0	-395.0	-380.27	-292.58					

Problem 2

This is similar to problem 1 except with two additional edge beams as shown in Fig. 5 . The beam is modeled by the stiffness matrix given in equation (12). Table 3 gives the "exact" values of the displacement components at the four ridge points of the mid-span section compared with those obtained from the finite element analysis using 154 elements for one half of the structure. Good agreement between results is noticed.

Table 3

Disp.	Ridge point 1		Ridge point 2		Ridge point 3		Ridge point 4	
Comp.	Exact	Finite El.	Exact	Finite El.	Exact	Finite El.	Exact	Finite El.
u	1.024	1.050	0.121	0.033	-0.406	-0.477	0.226	0.236 ft.
v	-40.09	-40.06	-1.552	- 1.215	-1.227	-1.180	6.154	6.470 ft.
w	-21.53	-21.30	0.938	1.138	2.302	2.071	-2.305	-2.338 ft.
θ_x	- 0.865	- 0.973	-1.789	- 1.663	0.635	0.617	0.191	0.206Rad.

* All values are multiplied by 10^{-4}.
* The two in-plane translations v and w at each of the ridge points are referred to the corresponding system of axes (Fig.5).

Problem 3:

Figure 6 shows the cross-section of a simply supported folded-plate roof with span of 32' and subjected to the given vertical loads. Results of the finite element analysis using a mesh of 120 elements for modeling one quarter of the structure, are shown in Fig. 7 for the longitudinal normal stress N_x, the transverse moment M_y, the transverse normal stress N_y at the mid-span section and the shear stresses N_{xy} at the section near the supports. Values obtained from the "exact" analytical solution by Leve are also plotted on the diagrams. The maximum difference between the values of the two solutions is less or equal to 4.3%, which is quite acceptable.

PRACTICAL APPLICATIONS

In order to study the effect of ; continuity, the type of intermediate supports, other elements such as beams and ties, on the behaviour of folded-plate structures, practical examples of three vents simply supported and continuous folded-plate roofs have been solved. The cross-section of these examples and the assumed case of vertical loading are given in Fig. 8. The first two examples are simply supported with span of 12 ms. The difference between the two examples is the addition of edge beams (20x40 cm section) at each of the bottom ridges in the second

example. The other three examples are continuous of two spans 12 ms each. While there are two end-diaphragms of 15 cm thickness in each of these cases, the condition at the intermediate support is different. In the first example, there is another 15 cm intermediate diaphragm supported on columns at the ridge points. In the second example, the diaphragm is substituted by (20x20 cm) ties connecting the columns top points. In the third example, the folded-plate is assumed to be directly supported on the column point supports at the ridge points. The number of elements used for modeling one quarter of the simply supported cases is 120. The elements used for discretizing one quarter of each of the three continuous cases are 264, 254 and 252 elements respectively.

Figures 9 a,b,c and 10 a,b,c give the distribution of the transverse moment M_y, the longitudinal and transverse normal stresses N_x and N_y at the mid-span section of the two simply supported cases. Figures 9d and 10d give the distribution of shear stresses N_{xy} at the end-supports in the two cases. From these diagrams, while values of the internal stresses in case of edge beams are generally decreased, the main reduction is in the positive values of N_x at the bottom ridges. Other values of stresses including the transverse moment M_y are slightly changed.

Figures 11a & b show the contour lines for the principal tensile stresses N_1 in the end and the intermediate diaphragms of the first case of the two spans examples. Figures 11c & d show the contour lines for N_1 in the end-diaphragms of the two other cases. The shape of the contour lines and the values of N_1 in the intermediate diaphragm explain the close behaviour of that case to the case of intermediate point supports connected with ties.

Distribution of N_{xy} over the section near the end-supports and that to the left of the intermediate supports in the three examples is shown in figures 12a & b. The increase of the values of N_{xy} at the end-supports and the corresponding increase in the values of N_1 in the end-diaphragms of the third case is due to the increase of the external reactions in this case compared to the other two cases. Also, the considerable increase in the external reactions at the intermediate supports in the case with an intermediate diaphragm, which reach almost four times the values of the end-reactions in that case, is responsible for the considerable increase in the shear stresses N_{xy} at that section and the increase in the principal tensile stresses in the intermediate diaphragm . Significant increase in the values of N_{xy} at the position of the intermediate point supports are also noticed. However, these values tend quickly to zero.

Figures 13a & b show the distribution of the transverse moment M_y at the mid-span section and the section at the intermediate support in the three examples. While the maximum values of M_y in the first two cases take place at section of 0.4 the span from the end-supports, in the case of inner point supports the maximum values are at the section of these supports. However, the difference between the maximum values of M_y and those at

the mid-span section in the first two cases is not significant. It is also noticed that the maximum values of M_y in the first two cases are less or equal to half those in the case of intermediate point supports, and that their values are less than those in the simply supported case by about 40%. While the values of M_y along any of the folds in the first two cases are always negative, in the third case M_y becomes positive at the outer upper fold of the first vent. This is due to the large transverse displacements of the section with intermediate point supports.

The distribution of the longitudinal normal stress N_x along each of the folds in the three examples is shown in Fig. 14. The maximum positive values of N_x are noticed to be at about 0.4 the span in the first case and at about half the span in the other two cases. These values in the first two cases are smaller than the corresponding values in the simply supported case by about 40%. The maximum positive values in the case of point supports are almost average values between those of the first two cases and the simply supported case.

Finally, the distribution of the transverse normal stresses N_y over the two sections of the mid-span and the intermediate supports is given in figures 15a & b . The values of N_y at the section of the point supports in the third case are 2-3 times those in the first case with intermediate diaphragm . The addition of ties reduces slightly these values.

From the above discussion, a great concentration of the transverse stresses M_y, N_y and N_{xy} at the position of the intermediate point supports is observed. However, the values of these stresses can be somewhat reduced if the actual cross-sectional dimensions of these columns are considered.

SUMMARY AND CONCLUSIONS

A finite element computer system for the general analysis of folded-plate structures has been developed. To show the effectiveness and versatility of the system to analyze large structures, practical examples have been solved. Based on the numerical results discussed in the paper, the following conclusions can be made:

1. Although values of the internal stresses are generally reduced by the addition of edge beams, the main reduction is in the positive values of the longitudinal normal stress N_x at the bottom ridges. Other values of stresses, including the transverse moment M_y, are slightly changed.
2. In case of continuous folded-plates with an intermediate diaphragm , the maximum positive values of N_x and the maximum values of the transverse moment M_y are reduced considerably compared to values for the simply supported case with similar span.
3. However, values of the shear stresses N_{xy} are somewhat increased at the inner intermediate diaphragm . This is due to

the considerable increase in the external reactions at the intermediate supports.

4. In case of inner point supports, a considerable increase in the values of the transverse stresses M_y, N_y and N_{xy} is noticed near these supports. This is attributed to the high values of concentrated reactions acting directly on the ridges and the big values of possible transverse relative displacements between the ridges at these supports.

5. Maximum positive values of the longitudinal stresses N_x in case of intermediate point supports are almost average values between those in the simply supported case and the continuous with an intermediate diaphragm .

6. The addition of ties connecting the top points of the intermediate columns in case of inner point supports reduces considerably all internal stresses and makes them almost approach the corresponding values in case of continuous with an intermediate diaphragm. However, some concentration in the transverse stresses N_y and N_{xy} at the point supports is still noticed.

REFERENCES

1. Hajdin, N., and Dunica, S., "Folded-Plates Stiffened by Diaphragms", Proceedings, Symposium on Folded-Plates and Spatial Structures, Udine, Italy, Sept. 23-27,1974.

2. Iffland, J.S., "Folded-Plate Structures", J. of Structural Div., ASCE, No. ST1, Jan., 1979.

3. Leve, H.Leon, "Theory of Folded-Plate Structures", A thesis Submitted for the Ph.D. degree, Purdue University, U.S.A.

4. Przemieniecki,J.S., "Theory of Matrix Structural Analysis", McGraw-Hill Book Company, 1968.

5. Rokey, K.C., and Evans, H.R., "A Critical Review of the Methods of Analysis for Folded Structures", Proceedings, Institute of Civil Engineers (London), Vol. 49, Part 2, June, 1971.

6. Zienkiewicz, O.C. (1971), "The Finite Element Method in Engineering Science", McGraw-Hill Publishing Company Limited, ENGLAND.

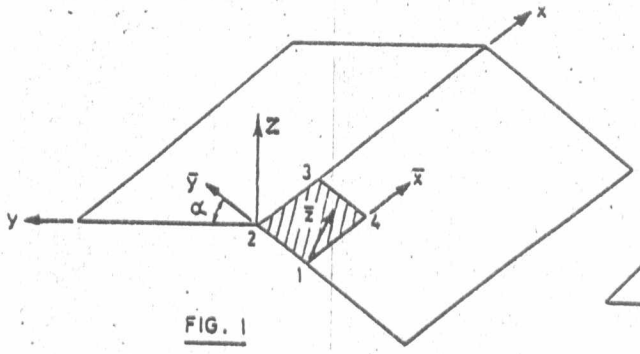

FIG. 1

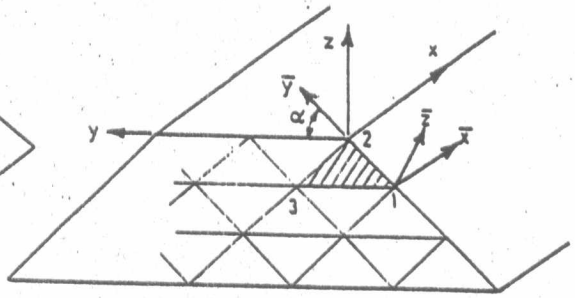

FIG. 2

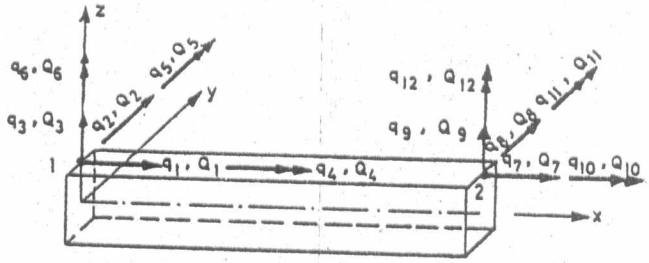

FIG. 3

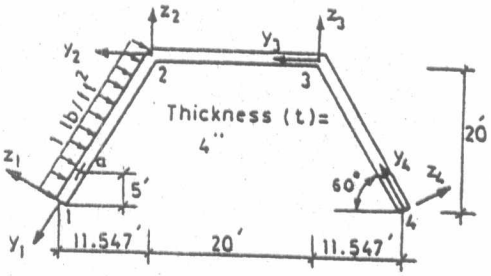

FIG. 4

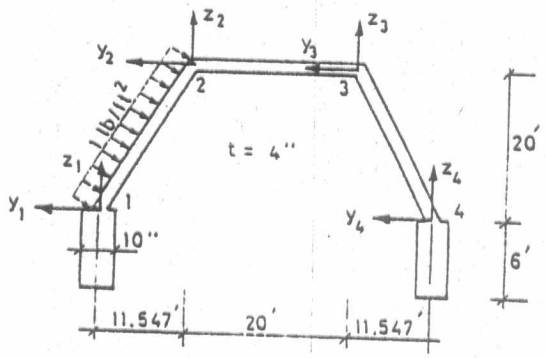

FIG. 5

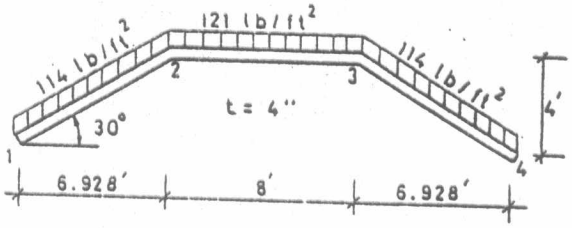

FIG. 6

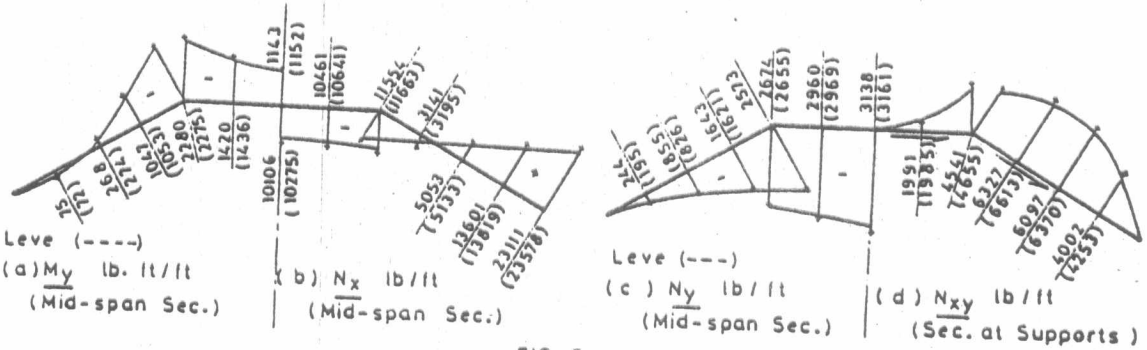

FIG. 7

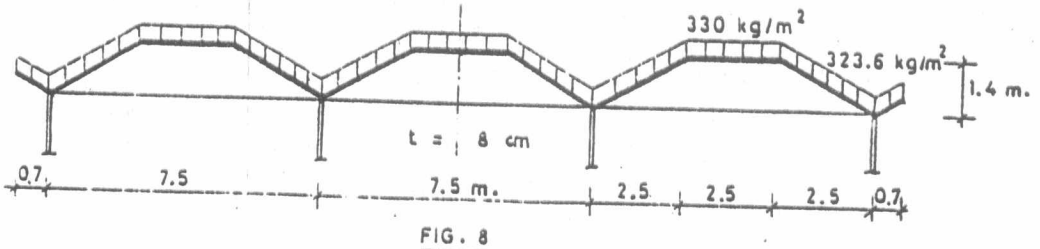

FIG. 8

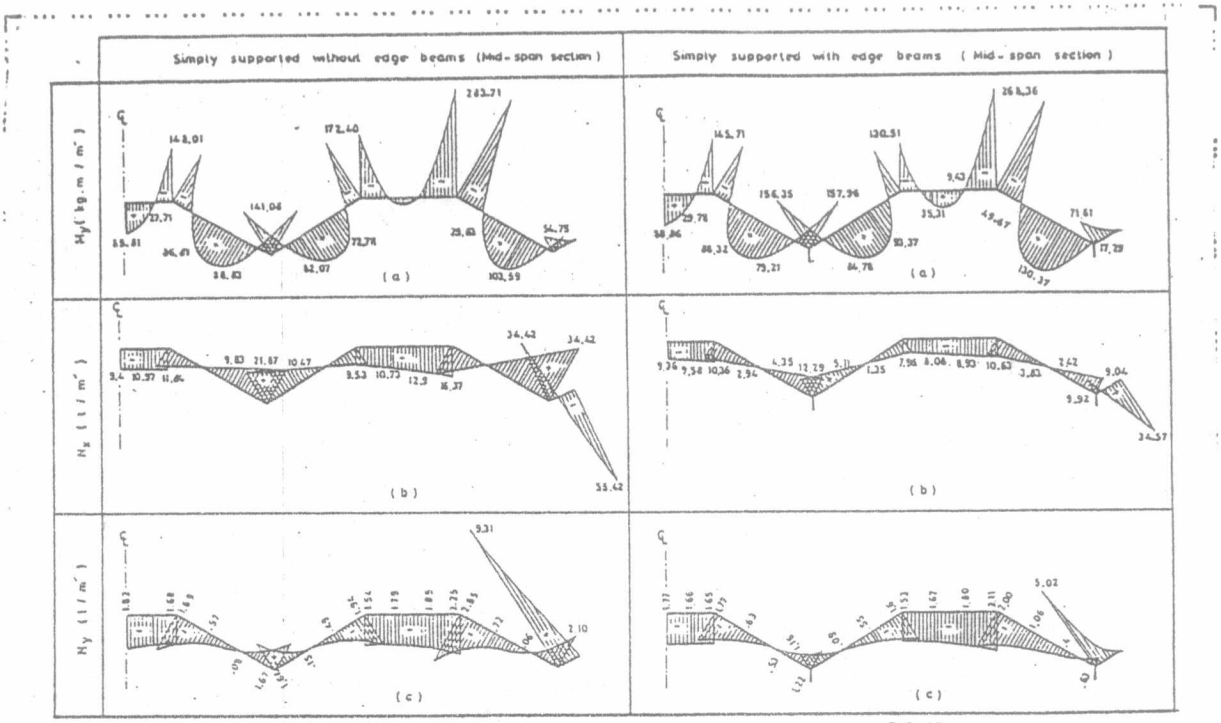

FIG. 9 a,b,c

FIG. 10 a,b,c

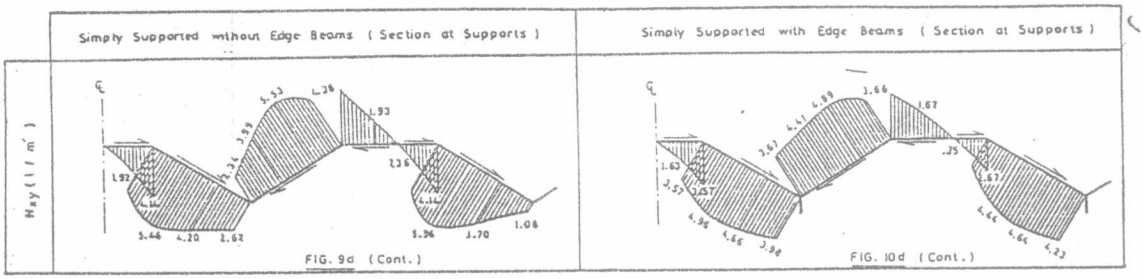

FIG. 9d (Cont.)

FIG. 10d (Cont.)

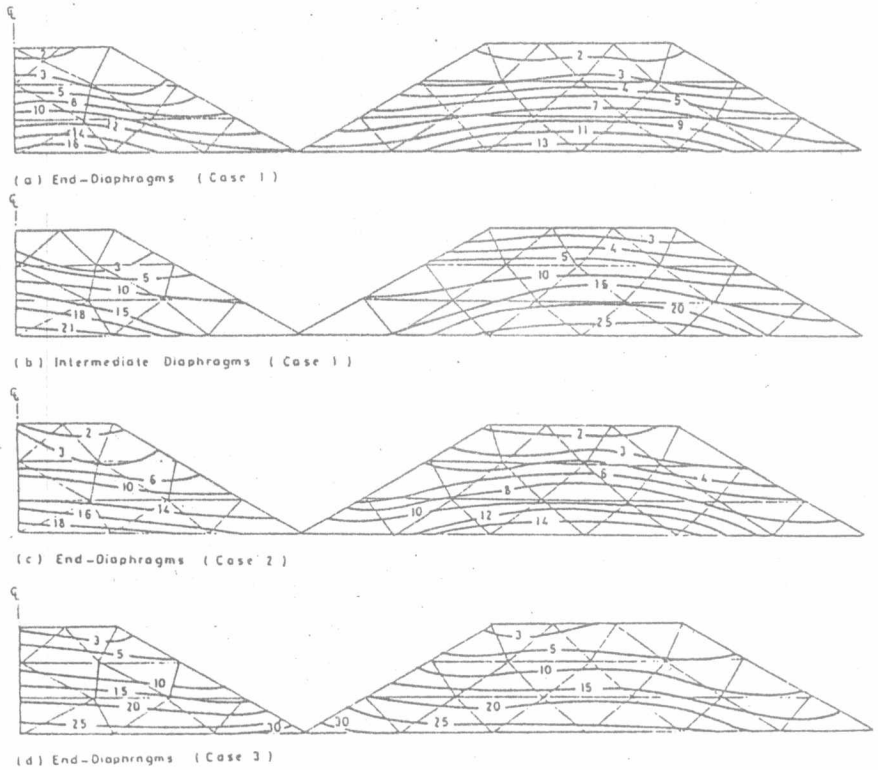

(a) End-Diaphragms (Case 1)

(b) Intermediate Diaphragms (Case 1)

(c) End-Diaphragms (Case 2)

(d) End-Diaphragms (Case 3)

FIG. 11 Contour Lines for N_1 Stresses in Diaphragms

6

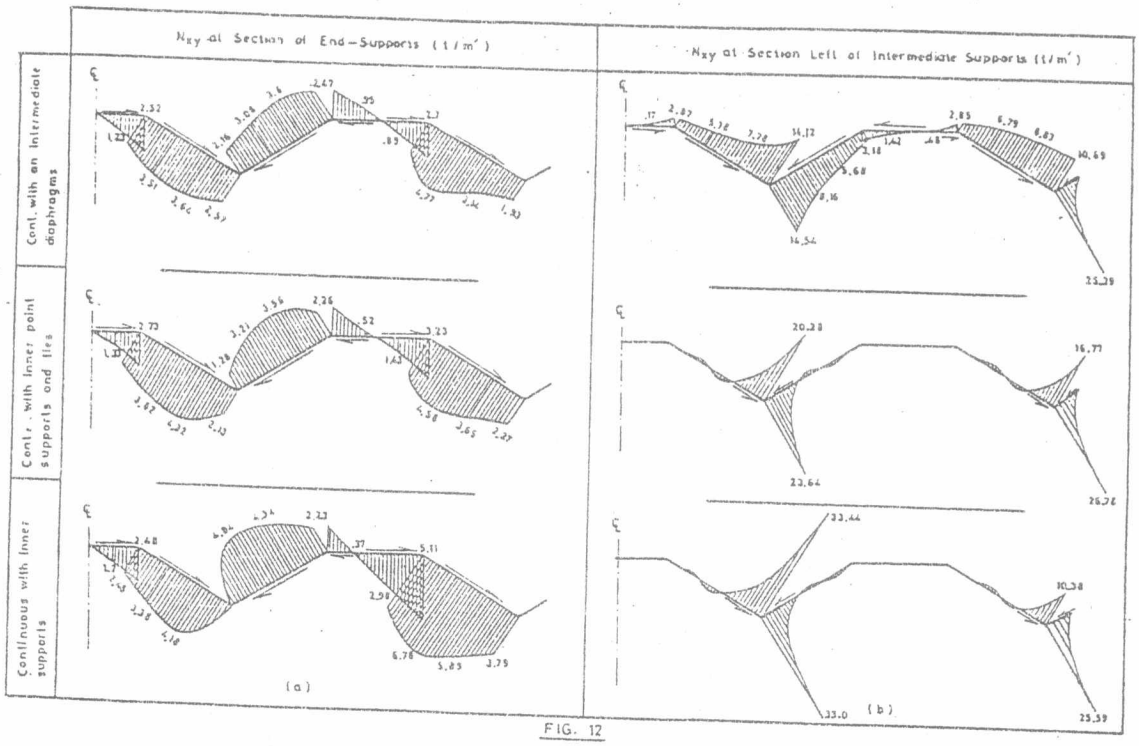

FIG. 12

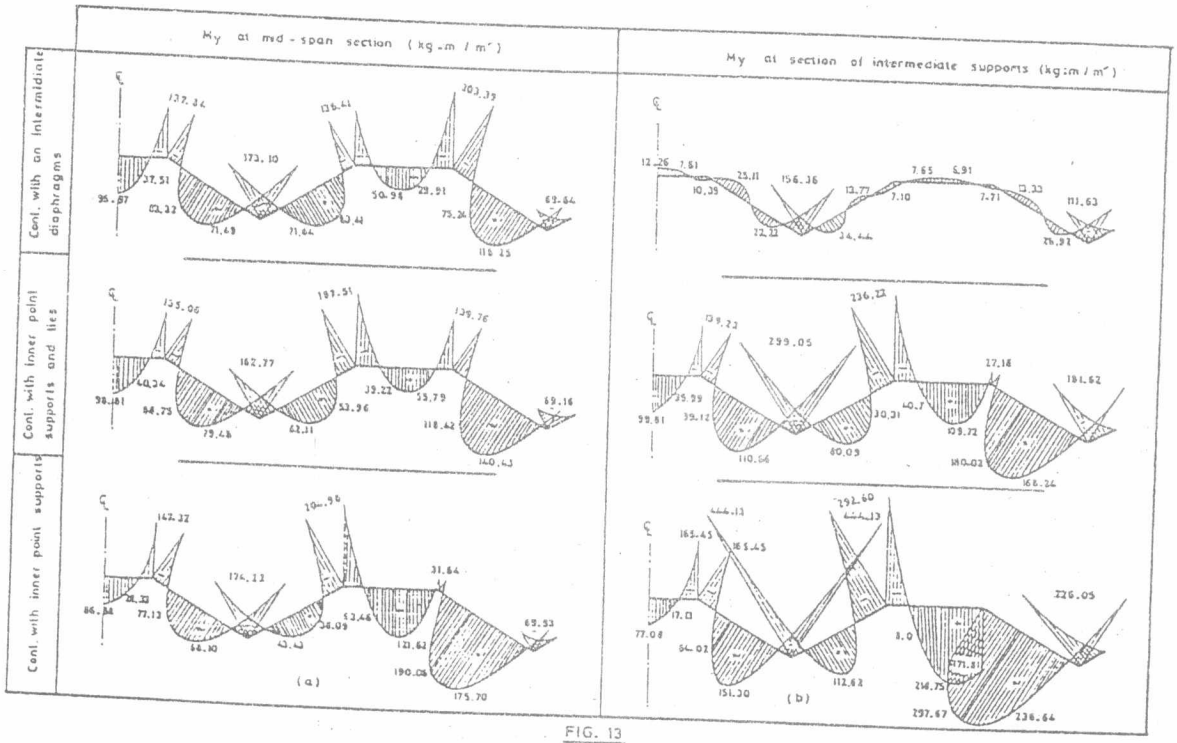

FIG. 13

6

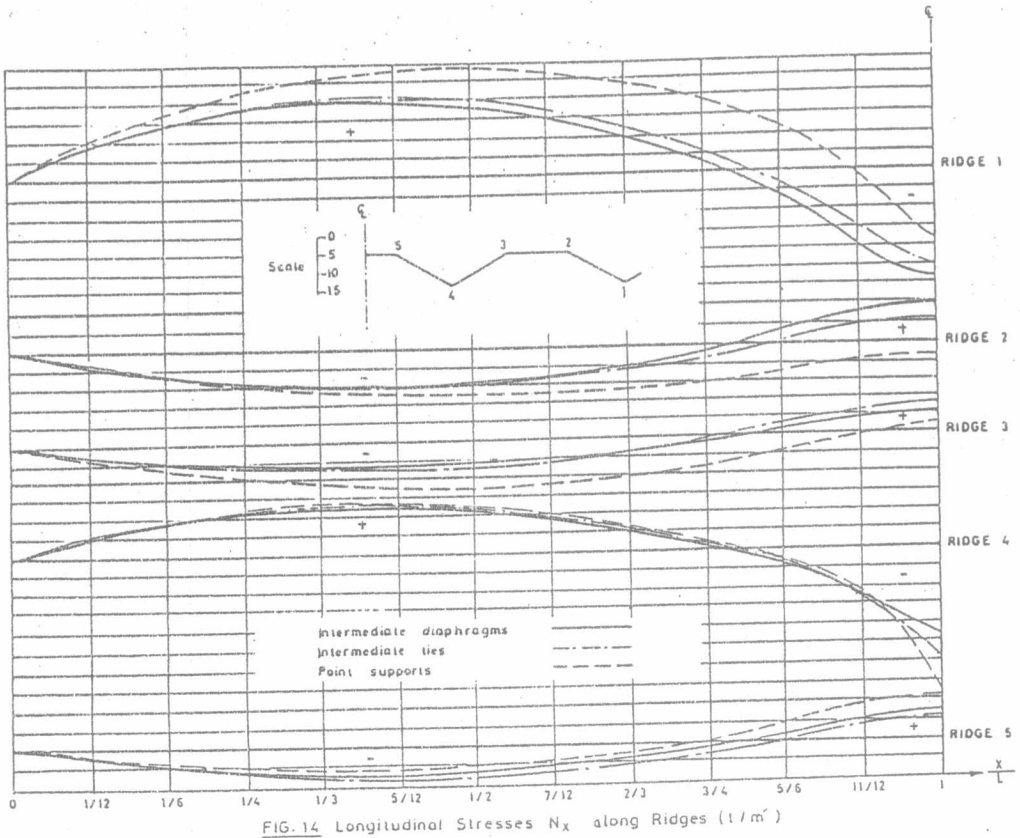

FIG. 14 Longitudinal Stresses N_x along Ridges (t / m')

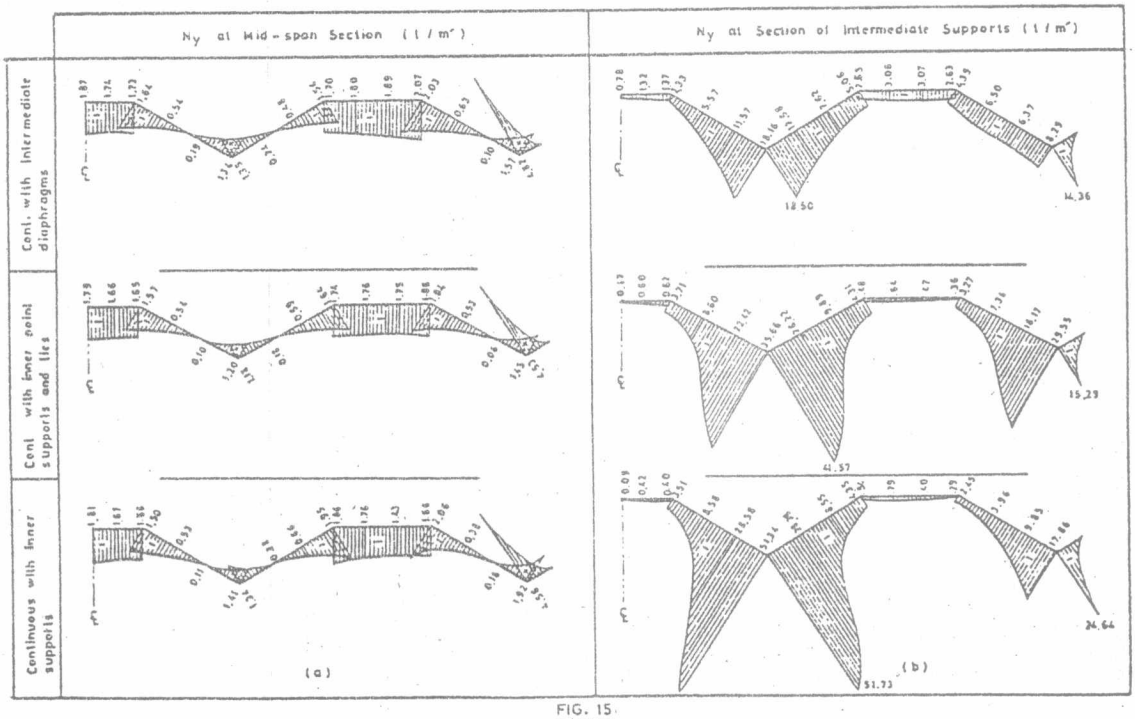

FIG. 15